WARWICK
THE UNIVERSITY OF WARWICK

Thermal Coupling Analysis in a Multi-chip Paralleled IGBT Module for a DFIG Wind Turbine Power Converter

Hui Li, Xinglin Liao, Zheng Zeng, Yaogang Hu, Yang Li, Shengquan Liu, and Li Ran, *Senior Member, IEEE*

Abstract—**Thermal coupling between adjacent IGBT or diode chips is the result of non-uniform temperature distribution in a multi-chip IGBT module. This affects the junction temperatures and hence the total power loss predicted for the module. The study first investigates the impact of thermal coupling effect on the junction temperatures through finite element method (FEM), and then develops a thermal coupling impedance model to represent such effect. The effect is shown to reduce with the distance exponentially. The model result agrees well with test. The validated model is then used to predict the junction temperature swings during operational power cycling in a DFIG wind turbine, showing the difference between the rotor and grid side converters. The model presented and the results obtained may be important for reliability evaluation and condition monitoring in the wind turbine power converters as well as in other multi-chip paralleled power electronic systems.**

Index Terms—**Doubly fed induction generator, wind turbine power converter, multi-chip paralleled IGBT module, thermal coupling impedance, junction temperature calculation.**

I. INTRODUCTION

Multi-chip paralleled insulated gate bipolar transistor (IGBT) power modules are widely used in wind turbine systems including offshore turbines [1–2]. The safe operation area (SOA) and reliability of the devices are highly dependent on the junction temperature. Thus, junction temperature evaluation and thermal modeling with respect to the intended operating conditions are important in design to guarantee the

Hui Li, Xinglin Liao, Zheng Zeng, Yaogang Hu and Li Ran are with the State Key Laboratory of Power Transmission Equipment & System Security and New Technology, School of Electrical Engineering, Chongqing University, Chongqing 400044, China (e-mail: cqulh@163.com; lxl108381@126.com; zengerzheng@126.com; huyaogang345@163.com; l.ran@warwick.ac.uk).

Yang Li is with the State Grid Chongqing Electric Power Co. Electric Power Research Institute, Chongqing, 401123, China (e-mail: 838147608@qq.com)

Shengquan Liu is with the State Grid Jiangxi Electric Power Corporation Ganzhou Power Supply Company, Ganzhou, 341000, China (e-mail: 840611955@qq.com).

Li Ran is also with the School of Engineering, the University of Warwick, Coventry, UK.

service lifetime reliability [3–4]. As reported in [5], nearly 60% of failures in electronic systems are associated abnormal temperatures, and the failure rate is almost doubled for every 10^0C increase of the junction temperature. However, it is difficult to know the actual junction temperature during operation and hence verify the model because of the sealed module packaging. In addition, most traditional thermal analysis models can not accurately calculate the junction temperatures in a multi-chip paralleled IGBT module due to simplification such as the ignorance of thermal coupling between the chips [6–7]. Given the strong dependence of power losses on the temperature itself, it may be crucial to take into account the thermal coupling effect within the multi-chip paralleled IGBT modules, for a more valid thermal analysis of wind turbine power converters.

It is challenging to establish an accurate model for the thermal behavior of a power device, especially for junction temperature evaluation in the context of reliability analysis. An FEM model was established to investigate the temperature distribution in an IGBT module in [8]. This method is time-consuming and could be unsuitable for analyzing a large number of transient scenarios. An infrared radiation thermal imaging technology for temperature testing was used in [9–10], but the method requires modification of the encapsulation, which is not allowed outside the laboratory. Various methods were proposed to construct a thermal impedance network to predict the chip temperatures [11–13]. However, their accuracy is always a concern, because the thermal coupling effect among chips in a multi-chips paralleled IGBT module is usually ignored. Alternatively, some experimental methods were proposed based on thermo-sensitive electrical parameters. For instance, the gate-emitter voltage (V_{ge}) was used to evaluate the chip temperature of multi-chip IGBT modules with thermal coupling [14–15], but it is difficult to detect the changes of V_{ge} during fast switching process. Furthermore, the method may also be invalid for multi-chip IGBT modules with non-uniform internal temperature distribution. Thus, for the purposes of safe operation and the improvement of reliability of wind turbine power converters, the thermal coupling effect in multi-chip paralleled IGBT module needs to be further investigated.

This paper presents a greatly improved thermal coupling impedance model to analyze the thermal coupling effect in multi-chip paralleled IGBT modules in the power converter of a

2MW doubly fed induction generator (DFIG) wind turbine system. In Section II, the thermal coupling phenomenon is investigated using FEM. In Section III, an improved thermal coupling impedance model is proposed and verified by the FEM results. In Sections IV and V, the junction temperature and the thermal coupling effect in the doubly fed induction generator wind turbine power converter are investigated as a case study. The presented model is compared to a traditional model and is also validated by the SCADA data from real operation

II. STRUCTURE OF IGBT MODULE FOR WIND TURBINE AND THERMAL COUPLING DESCRIPTION

To investigate the thermal coupling effect, a multi-chip paralleled IGBT module, FZ1600R17HP4, that is widely used in doubly fed induction generator wind turbine power converters is considered. The power converter and the module structure are shown in Fig. 1.

Fig. 1(a) shows that each half-bridge module consists of 16 IGBT and 16 free-wheeling diode (FWD) chips covered with silica gel. The packaging structure is divided into seven layers from a cross-sectional point of view, as shown in Fig. 1(b). The two copper layers of the direct bonded copper (DBC) are connected to the devices and the base plate respectively using solder. Because all chips are fixed on a single base plate, the heat coming from one chip will affect the others, which would affect the accuracy of device modeling.
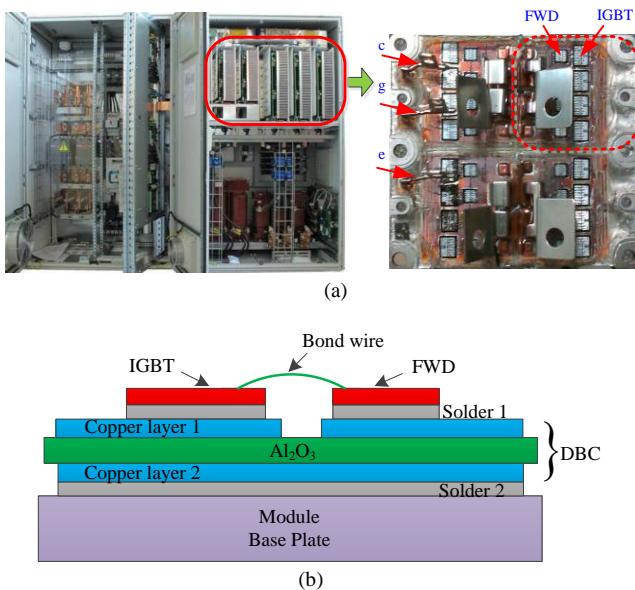

(a)

(b)

Fig. 1 Structure of IGBT module with multiple chips.(a) IGBT module in converter and (b) cross-section view of module packaging structure.

Because of the symmetrical structure shown in Fig. 1(a), a 1/4 unit marked as T1–T4 and D1–D4 of the whole power module is chosen in the study, and this is shown in Fig.2. The dimensions of and distances between the chips are shown in the figure. Chips T1, T4, D1, and D4 are the edge, whereas the others are the central chips.

The material characteristics of each packaging layer of the FZ1600R17HP4 module are shown in Table I [16].

Assumptions are made as follows: 1) there is no effect of different chip temperatures on the dynamic current sharing [7]; 2) each layer is connected perfectly without relative movement; 3) there is no heat spreading through the silica gel; 4) all heat comes from the active junctions and flows to the cooling air below the heat-sink; 5) the ambient temperature is 50 ℃; 6) there is no effect of bond wires or internal bus bars on the temperature[17].
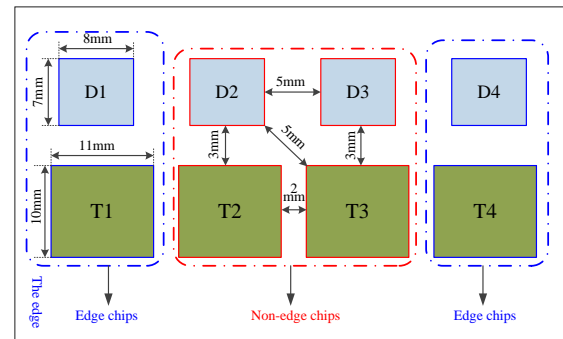
Fig. 2 Chip size of IGBT module for wind power converter

TABLE I
MATERIAL PROPERTIES OF IGBT MODULES

IGBT module	Material	Thermal Conductivity /W·(m·K)$^{-1}$	Height/mm	Mass Density /kg·m^{-3}
IGBT	Si	139	0.3	2329
FWD	Si	139	0.3	2329
Solder1	Sn-Ag-Cu	78	0.05	7400
DCB Copper1	Cu	386	0.3	8960
Ceramic	Al$_2$O$_3$	18	0.7	3690
DCB Copper2	Cu	386	0.3	8960
Solder2	Sn-Ag-Cu	78	0.1	7400
Base Plate	Cu	386	3	8960

Based on these, a 3D finite element model of the multi-chip paralleled IGBT module is established using ANSYS, as shown in Fig. 3(a). When 2.27 W/mm^3 power losses are injected into each of chips T1–T4, the temperature distribution of chips T1–T4 is shown in Fig.3 (b).

(a)

This article has been accepted for publication in a future issue of this journal, but has not been fully edited. Content may change prior to final publication. Citation information: DOI 10.1109/TEC.2016.2614526, IEEE Transactions on Energy Conversion

3
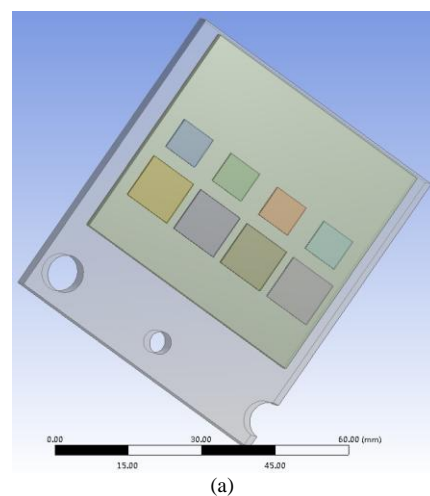
Fig. 3 3D model and thermal profile of multi-chip paralleled IGBT module (a) 3D finite element model and (b) steady thermal profile under the injected 2.27w/mm³ power loss condition

Fig. 3(b) shows that the maximum junction temperature of the IGBT module is about 103.53 ℃ on chip T2. In addition, the thermal distributions of chips T1 to T4 are also different. The areas with temperature ranging from 97.888 ℃ to 103.53 ℃ on chips T2 and T3 are wider than those on chips T1 and T4; the max maximum junction temperatures are also different. As mentioned previously, the reason is likely to be the thermal coupling effect among the chips. Because junction temperature is important for device selection, heat sink design and condition 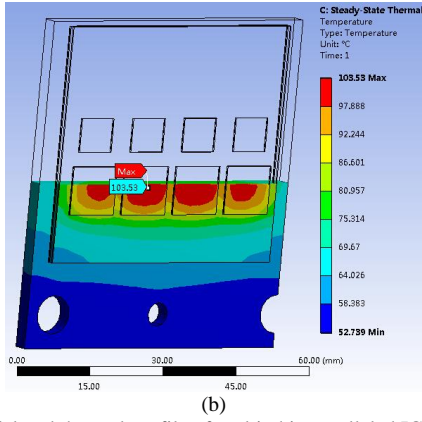monitoring of the converter, it is necessary to establish a more accurate calculation model of the junction temperatures by considering the thermal coupling effect. In order to accurately describe the thermal coupling effects among the chips, a coupling junction temperature concept is established in the following section, i.e., the maximum steady-state junction temperature when power losses are injected into the nearby chips.

III. THERMAL COUPLING EFFECT AND IMPROVED THERMAL COUPLING IMPEDANCE MODEL

A. Improved Thermal Coupling Impedance Model

The thermal problem for a typical power module can be reduced to a thermal diffusion process, which is dominated by heat conduction[18]. In a homogeneous isotropic material, the heat conduction equation is described as:

$$\nabla(\kappa\nabla T) = H + \rho c \frac{\partial T}{\partial t} \tag{1}$$

where k is the thermal conductivity, H is a position dependent volumetric heat source, ρ is the mass density, c is the specific heat capacity. Usually the heat sources are the semiconductor dies and can be treated as sources of surface heat flux, the heat conduction equation simplifies to [19]

$$\kappa(\frac{\partial^2 T}{\partial x^2} + \frac{\partial^2 T}{\partial y^2} + \frac{\partial^2 T}{\partial z^2}) = \rho c \frac{\partial T}{\partial t} \tag{2}$$

where x, y, z denote the directions of heat propagation in space. As is known to all, IGBT is a vertical power device and its thickness is small compared to other dimensions. The heat is generally dissipated uniformly across the surface of the chips and flows vertically toward the heat sink. Fig.4 shows the heat dissipation path in IGBT module.
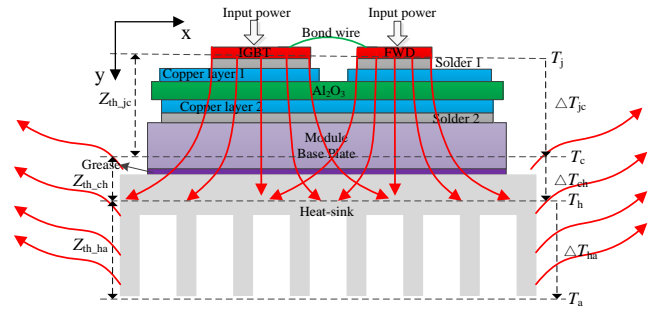
Fig. 4 The path of heat dissipation in IGBT module
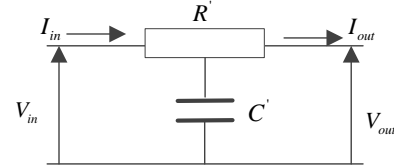
Fig. 5 A section of an *RC* ladder network in a transmission line model
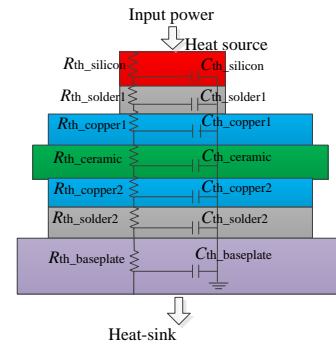
Fig.6 Thermal *RC* network for a single chip

In addition, the effect of temperature on the thermal conductivity of a silicon chip can be ignored. Thus, the heat conduction process can be treated as a quasi-one-dimensional process and equation (2) can be further simplified to:

$$\kappa \frac{\partial^2 T}{\partial y^2} = \rho c \frac{\partial T}{\partial t} \tag{3}$$

with boundary conditions,

$$S\kappa \frac{\partial T}{\partial y}\Big|_{y=0} = -P_{in} \text{ and } T(t, y = L) = T_a \tag{4}$$

where P_{in} is the input power, S the area perpendicular to the heat conduction direction y, L is the vertical length along y direction and T_a the ambient temperature.

In the electric domain, the wave equation of a transmission line for the potential V can be described with the distributed capacitance C' and distributed resistance R', which can be written as[20]:

$$\frac{\partial^2 V}{\partial x^2} = C'R' \frac{\partial V}{\partial t} \tag{5}$$

Fig.5 shows schematically a section of a transmission line based on equation (5), which is the building block an *RC* ladder network. Similarly, for an IGBT module, a similar transmission line equivalent circuit format can be adopted to describe the heat conduction path. The power dissipated by an IGBT (or a diode) is regarded as a heat source in the thermal circuit. 'C''

and 'R'' denote the thermal resistance and thermal capacitance which are usually labeled as 'R_{th}' and 'C_{th}' in a thermal network, respectively.

Fig. 7 Simplified external characteristic equivalent thermal RC network between junction and case layer

As shown in Fig.1, the IGBT module consists of seven layers, which is further connected to the heat-sink. The thermal property of each layer can be described by a lumped RC ladder network with thermal resistance and thermal capacitance shown in Fig.5.The following equations are used to estimate the thermal resistance and capacitance of each layer:
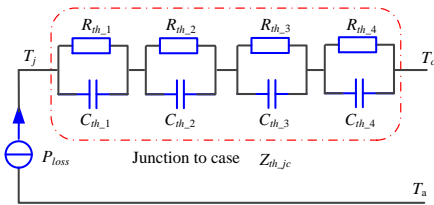
$$R_{th}=\frac{d}{A \cdot \kappa} \qquad C_{th}=c \cdot \rho \cdot d \cdot S \qquad (6)$$

where d is the thickness of each layer. It is known from Fig.6 that the thermal property parameters such as R_{th} and C_{th} of each layer are needed in the RC network, but it is not straightforward to obtain these parameters. In order to simplify, a 4th order Foster characteristic equivalent circuit is adopted to adequately describe the thermal property of IGBT module from junction to case[12,13], as shown in Fig.7. The Forster-based junction temperature calculation model is also called the traditional model used widely, which is compared with the improved thermal coupling model in the following section.

TABLE II
PARAMETERS OF RC NETWORK OF FIG.7

Chip	Thermal impedance	i			
		1	2	3	4
IGBT	R_{th_i}(K/kW)	1.131	11.42	1.482	0.537
	C_{th_i}(J/K)	1.415	3.52	176.788	7178.77
FWD	R_{th_i}(K/kW)	1.621	2.352	18.53	1.84
	C_{th_i}(J/K)	0.37	1.91	2.08	299.46

Due to the self-heating of chips resulting from the power loss P_{loss}, the transient thermal impedance between junction to case layer is defined at time t as

$$Z_{th\_jc}=\frac{T_j(t)-T_c(t)}{P_{loss}}=\frac{\Delta T_{jc}}{P_{loss}} \qquad (7)$$

The transient thermal impedance between the case and heat-sink layer (Z_{th_ch}) and the heat-sink itself (Z_{th_ha}) can be obtained similarly, as shown in Fig.4. From a circuit point view, the transient thermal impedance curve is a step response curve with zero-initial conditions and can be fitted into a finite series of exponential terms:

$$Z_{th\_jc}=\sum_{i=1}^{n}R_{th\_i}(1-e^{-t/\tau_{th\_i}}) \ , \ (\tau_{th\_i}=R_{th\_i}C_{th\_i}) \qquad (8)$$

where τ_{th} is the time constant. In Fig.7, each of the thermal parameters can be found from the manufacturer datasheets for the module, which are listed in Table II. Based on the Fig.7 and

Table II, Z_{th_jc} for IGBT and FWD can be calculated approximately as

$$Z_{IGBT\_th\_jc}=\sum_{i=1}^{4}R_{th\_i}(1-e^{-t/\tau_{th\_i}})=10^{-3}\times(1.131\times(1-e^{-t/0.0016})+$$
$$11.42\times(1-e^{-t/0.0402})+1.482\times(1-e^{-t/0.0262}) \qquad (9)$$
$$+0.537\times(1-e^{-t/3.855}))$$

$$Z_{FWD\_th\_jc}=\sum_{i=1}^{4}R_{th\_i}(1-e^{-t/t_{th\_i}})=10^{-3}\times(1.621\times(1-e^{-t/0.0006})+$$
$$2.352\times(1-e^{-t/0.0045})+18.53\times(1-e^{-t/0.0368}) \qquad (10)$$
$$+1.84\times(1-e^{-t/0.551}))$$

It is assumed that the number of chips is n, a self-thermal impedance matrix method is adopted as follows.

$$\mathbf{Z}_{self}=\begin{bmatrix} Z_{th\_jc1} & 0 & \cdots & 0 \\ 0 & Z_{th\_jc2} & \cdots & 0 \\ \vdots & \vdots & \vdots & \vdots \\ 0 & 0 & \cdots & Z_{th\_jcn} \end{bmatrix} \qquad (11)$$

Fig.8 shows the simplified heat flow paths inside the IGBT module. Because different chips share the same DBC and base plate in a multi-chip IGBT module, the existence of thermal coupling is inevitable, as shown above in part II.
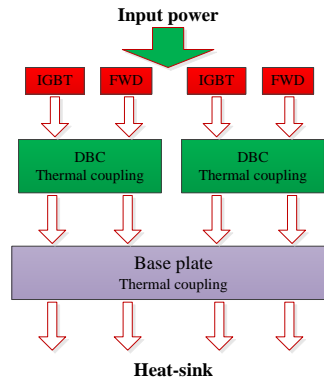
Fig. 8 Simplified heat flow paths inside the IGBT module

A transient equivalent thermal coupling impedance is introduced to describe the increment of the maximum junction temperature of the concerned chip caused by the power loss of a neighboring chip and is defined at time t as

$$Z_{thc(n,m)}=(T_{jn}(t)-T_a(t))/P_{loss\_m} \qquad (12)$$

where $Z_{thc(n,m)}$ is the transient equivalent thermal coupling impedance between chips n and m , T_{jn} the maximum junction temperature increment of chip n generated by the power loss P_{loss_m} of chip m, T_a the ambient temperature.

In this way, a thermal coupling impedance matrix method is also adopted to describe the thermal coupling effects among chips as

$$\mathbf{Z}_{couple}=\begin{bmatrix} 0 & Z_{thc(1,2)} & \cdots & Z_{thc(1,n)} \\ Z_{thc(2,1)} & 0 & \cdots & Z_{thc(2,n)} \\ \vdots & \vdots & \vdots & \vdots \\ Z_{thc(n,1)} & Z_{thc(n,2)} & \cdots & 0 \end{bmatrix} \qquad (13)$$

This article has been accepted for publication in a future issue of this journal, but has not been fully edited. Content may change prior to final publication. Citation information: DOI 10.1109/TEC.2016.2614526, IEEE Transactions on Energy Conversion

5

where $Z_{th(1,2)}$ is the thermal coupling impedance between chips 1 and 2, which is caused by chip 2. According to the above analysis, the improved thermal coupling impedance model is derived as shown in Fig.9. Thus, the junction temperature considering the multi-chip thermal coupling effects can be calculated by equation (14).

Fig. 9 Improved thermal coupling impedance model of IGBT module

$$\begin{bmatrix} T_{j1} \\ T_{j2} \\ \vdots \\ T_{jn} \end{bmatrix} = \begin{bmatrix} Z_{th\_jc1} & Z_{thc(1,2)} & \cdots & Z_{thc(1,n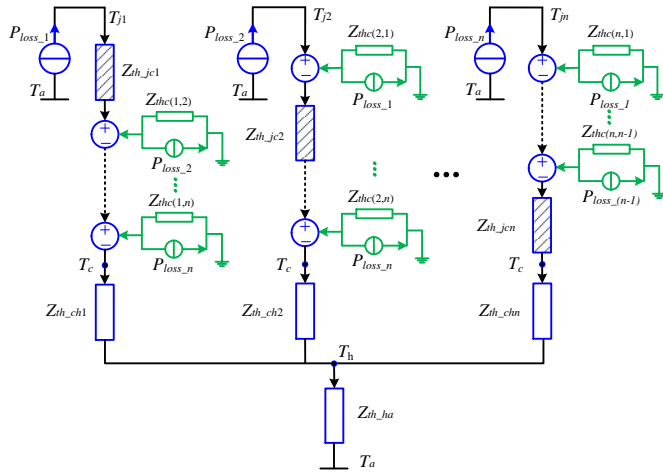)} \\ Z_{thc(2,1)} & Z_{th\_jc2} & \cdots & Z_{thc(2,n)} \\ \vdots & \vdots & \vdots & \vdots \\ Z_{thc(n,1)} & Z_{thc(n,2)} & \cdots & Z_{th\_jcn} \end{bmatrix} \cdot \begin{bmatrix} P_{loss\_1} \\ P_{loss\_2} \\ \vdots \\ P_{loss\_n} \end{bmatrix} + \begin{bmatrix} P_{loss\_1} \\ P_{loss\_2} \\ \vdots \\ P_{loss\_n} \end{bmatrix} \cdot$$

$$\begin{bmatrix} Z_{th\_ch1} & Z_{th\_ch2} & \cdots & Z_{th\_chn} \end{bmatrix} + \sum_{i=1}^{n} P_{loss\_i} \cdot Z_{th\_ha} + T_a \qquad (14)$$

The temperature as a function of time can be obtained by ANSYS for a given power loss excitation. And then, according to equation (12), thermal coupling impedance Z_{thc} as a function of time can also be acquired. Similarly the curve fitting method is also applied to the acquired transient thermal coupling impedance data as:

$$Z_{thc}(t) = R_{thc}(1 - e^{-t/\tau_{thc}}) \quad , \quad (\tau_{thc} = R_{thc}C_{thc}) \qquad (15)$$

where τ_{thc} is the thermal coupling time constant, R_{thc} and C_{thc} are the coupling thermal resistance and capacitance, respectively. Based on this method, the thermal coupling impedance can be easily extracted. Table III shows the extracted thermal coupling impedance parameters for chips T1–T2 and D1–D2 shown in Fig. 2.

TABLE III
THE COUPLING THERMAL IMPEDANCE OF IGBT MODULE

Chip number		T1	T2	D1	D2
	T1	-	(0.0251,99)	(0.0124,290)	(0.0074,540)
Z_{thc}	T2	(0.0255,98)	-	(0.0081,493)	(0.0128,281)
(R_{thc}, C_{thc})	D1	(0.0129,279)	(0.0083,481)	-	(0.0041,980)
	D2	(0.0069,579)	(0.0124,290)	(0.0045,933)	-

Theoretically, the thermal coupling impedances between two chips should be the reciprocals, but there is a little difference as shown in Table III, which would be caused by the extracted

values from the FEM. As seen in Fig.10, it is shown that the thermal coupling impedance between chips T1 and T2 as a function of the distance exhibits an approximately exponential characteristic, which decreases with the increasing distance. When the distance is more than 10 mm, their coupling thermal effect may be ignored.
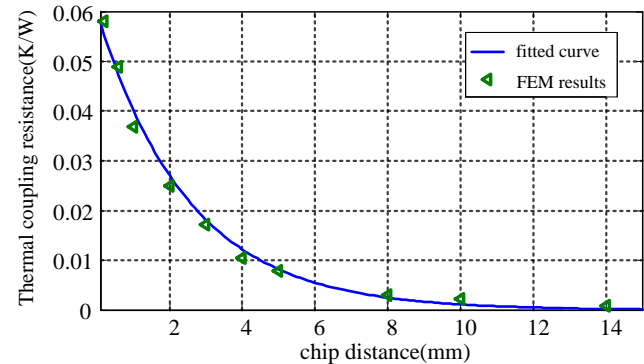

Fig. 10 The coupling thermal resistance versus distance between chips

The heat sink is assumed to be at a uniform temperature. The thermal capacitance in Z_{th_ch} is assumed to be negligible, and the thermal resistances are selected as 9.75 K/kW and 10.5 K/kW for IGBT and FWD, respectively. The thermal resistance and thermal capacitance for the heat-sink are selected as 80 K/W and 1320.8 J/K. Through the analyses above, the junction temperature of any one chip can be calculated more accurately based on the proposed model. For example, when the junction temperature of chip 2 is calculated, chips 1 and chips 3–n ($n=4$ in the case described above) need to be considered as the adjacent thermal sources because of the thermal coupling effect. However, because the thermal coupling resistance decreases with the increase of the distance in FZ1600R17HP4, and the effect can be ignored at a distance in excess of 10 mm as shown in Fig.10, the junction temperature of chip T2 only needs to consider the thermal coupling effects of chips T1, T3 and D1. The distinction between the proposed model and the traditional foster thermal model is whether to consider thermal coupling effect of the nearby chips. Thus, the junction temperature and hence the device power losses using the proposed model would be more accurate.

B. Simulation comparison of different thermal models

To demonstrate the validity of the improved junction temperature calculation model, a comparison with FEM is first performed for the traditional Foster model and the improved model. For the structure of the IGBT module in the 2 MW DFIG wind turbine system, as shown in Fig. 1, the distance between each 1/4 of the IGBT/FWD pairs of the whole module is more than 10 mm. Hence, the 1/4 unit of the IGBT module is chosen in the thermal coupling analysis. The mean values of the injected power loss are 150 W and 120 W for IGBT and FWD, but the transient power losses that are calculated using the switching period method in [21] are injected into chips T1–T4 and D1–D4 for ANSYS simulation by using its transient thermal analysis tool. The junction temperatures of chips T1 and T2 with different thermal models are shown in Fig. 11.
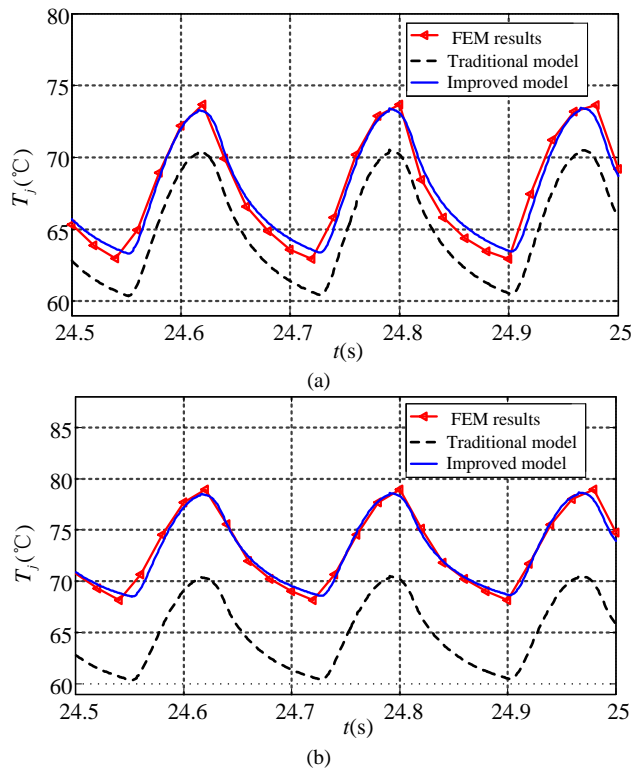
Fig. 11 Comparison of different junction temperature models with FEM (a) junction temperature of chip T1 and (b) junction temperature of chip T2

The comparison shows good agreement between the improved model and FEM results and the improved thermal model gives more satisfactory results as compared to the traditional thermal network model. Furthermore, the junction temperature obtained by the traditional model is lower than that by the FEM method and the improved model, suggesting that the temperatures and hence losses of chips tend to be under-estimated in the traditional model. Therefore, the proposed method could be more suitable for multi-chip paralleled IGBT modules. It is also noticed that the effect of thermal coupling on the magnitude of junction temperature is pretty obvious, but for the peak-peak fluctuation magnitude and frequency, there is almost no effect. The differences between the traditional and improved models, measured in junction temperatures are about 3 ℃ and 8 ℃ for chips T1 and T2 respectively, which would be larger as the power loss increases and might have a significant effect on the operational reliability evaluation of the large wind turbine power converters.

Given thermal coupling being significant, the following section will further analyze the junction temperature calculation and the coupling characteristics of chips T2 and D2 in the multi-chip paralleled IGBT module as used in a doubly fed wind turbine power converter.

IV. Case Study of a 2 MW Wind Turbine Power Converter

A. Description of DFIG wind turbine

Due to the variable speed constant frequency characteristics of wind turbines, the operational performance and the reliability requirement for IGBT may be different to the traditional driver system. In addition, the rated capacity of the installed on-shore wind turbine is mainly around 1.5-2MW. Furthermore, in the current 2 MW DFIG wind turbine system, the IGBT module type of FZ1600R17HP4 with the multiple chips has been used widely. Taken as an example, a 2 MW DFIG wind turbine system is chosen to verify the significance of the proposed model. This mechanical power is [21]

$$P_{mech} = \frac{1}{2}\rho A C_p(\lambda, \beta) v_w^3 \qquad (16)$$

where ρ is the air density, A the area swept by the turbine blades, and v_w the wind velocity. β is the blade pitch angle, and λ is the tip speed ratio. C_p is the transfer efficiency.

Fig. 12 shows such a system. The electrical part of the DFIG wind turbine consists of a wound-rotor induction machine. The stator terminals are directly connected to the medium voltage (MV) grid via a three-winding transformer. The rotor is excited by a power electronic converter, which consists of two AC-DC converters named rotor-side converter (RSC) and grid-side converter (GSC) in a back-to-back configuration with a common DC-link bus. The GSC feeds the rotor power into the grid via an LCL filter and the tertiary winding of the transformer.
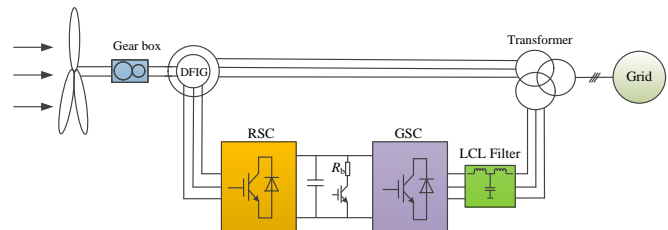

Fig. 12 Diagram of a doubly fed wind turbine system

The RSC regulates the torque of the DFIG and the rotational speed usually using a double loop controller where the outer speed loop generates the reference signal for the inner current loop. The current control is conducted in the synchronous reference framework (d-q) rotating with the stator flux [22]. The GSC maintains the DC-link voltage and by doing so transfers the active power from the RSC into the grid, which will inevitably produce power losses in the power semiconductor modules.

TABLE IV
PARAMETERS OF A REAL 2MW DFIG WIND TURBINE SYSTEM

Parameters	Value	Parameters	Value
Rated power	2 MW	Stator resistance R_s	0.022 Ω
Rated voltage	690 V	Stator leakage inductance L_{ls}	0.012 mH
Rated wind speed	12 m/s	Rotor resistance R_r	0.0018 Ω
Cut-in wind speed	3 m/s	Rotor leakage inductance L_{lr}	0.05 mH
Cut out wind speed	25 m/s	Mutual inductance L_m	2.9 mH
Synchronous speed	1500 rpm	Pole Pairs	2
Cooling system	air cooling	Rated frequency	50 Hz
Modulation technique	SVPWM	DC bus voltage	950 V
Rotor rotational inertia	75kg·m²	Turn ratio	0.3774
Reactive power at grid and rotor side	0 Var	Wind speed at synchronous speed point	9.32 m/s
Starting point wind speed at constant power range	12 m/s	Starting point wind speed at constant rotation rate range	11.3 m/s
Switching frequency of RSC	2000 Hz	Switching frequency of GSC	4000 Hz

As shown in Fig. 12, the rotor terminals of the DFIG are directly connected to the RSC and the stator terminals are connected to the GSC via the three-winding transformer and LCL filter. In general, the frequency of current (or voltage) in stator winding is higher than that in rotor winding. So, in order to reduce the harmonics, the switching frequency of GSC is higher than that of RSC; the switching is set at 4000 Hz and 2000 Hz for the GSC and RSC respectively in this 2 MW DFIG wind turbine as shown in Table IV. Other parameters of DFIG wind turbine system, such as, modulation technique, cooling ystem, turns ratio, DC bus voltage, reactive power at grid and rotor sides, pole pairs, etc., are also shown in Table IV.

B. Power losses of IGBT modules

The semiconductor power losses are very important for thermal design of the converter, which is mainly composed of switching and conduction losses. The conduction loss, which is related to conduction voltage drop, current, duty cycle, and junction temperature, can be derived as the equations below [23].

$$P_{Ic} = \begin{cases} \delta_{(t)}(v_I \cdot i_{(t)} + r_I \cdot i_{(t)}^2) & i(t) > 0 \\ 0 & i(t) \le 0 \end{cases} \quad (17)$$

$$P_{Dc} = \begin{cases} (1-\delta_{(t)})(v_D \cdot i_{(t)} + r_D \cdot i_{(t)}^2) & i(t) > 0 \\ 0 & i(t) \le 0 \end{cases} \quad (18)$$

where P_{Ic} denotes the IGBT conduction loss, P_{Dc} denotes the FWD conduction loss; v_I and v_D are the conduction and forward voltage drops for the IGBT and FWD, respectively; r_I is the conduction resistance for the IGBT and r_D is the conduction resistance for FWD, i(t) is the output current of the converter, and δ(t) is the duty ratio of IGBT, which is calculated as follows

$$\delta_{(t)} = \frac{1 \pm m \cdot \sin(\omega t + \phi)}{2} \quad (19)$$

where sign '+' is used for the inverter and '-' for the rectifier mode, m is the modulation index, ω the angular frequency; and ϕ the phase angle between voltage and current.

Switching losses are related to the switching frequency and the current of the converter as well as the junction temperature, which can be expressed as [22]

$$P_{Is} = \begin{cases} f_s \cdot (E_{on} + E_{off}) \cdot (V_{dc} \cdot i(t))/(V_n \cdot I_n) & i(t) > 0 \\ 0 & i(t) \le 0 \end{cases} \quad (20)$$

$$P_{Ds} = \begin{cases} f_s \cdot (E_{rec}) \cdot (V_{dc} \cdot i(t))/(V_n \cdot I_n) & i(t) > 0 \\ 0 & i(t) \le 0 \end{cases} \quad (21)$$

where P_{Is} is the switching loss of an IGBT and P_{Ds} the switching loss of a FWD; f_s is the switching frequency, while E_{on} and E_{off} are the turn-on and turn-off energy losses at rated operation condition respectively; V_{dc} is the DC-link voltage of converter, V_n and I_n are the rated voltage and rated current of IGBT, and E_{rec} is the diode reverse recovery losses.

C. Junction temperature calculation for IGBT module in wind power converters

Fig. 13 shows the calculation flowchart of the junction temperature and case temperature (assumed to be uniform) of the multi-chip paralleled IGBT module for the 2MW DFIG wind power converter in concern. Incorporating the model developed in this study, the junction temperatures and case temperature can are calculated via the software platform PLECS. A traditional control model is used for the DFIG system over a full range of the intended operating point.
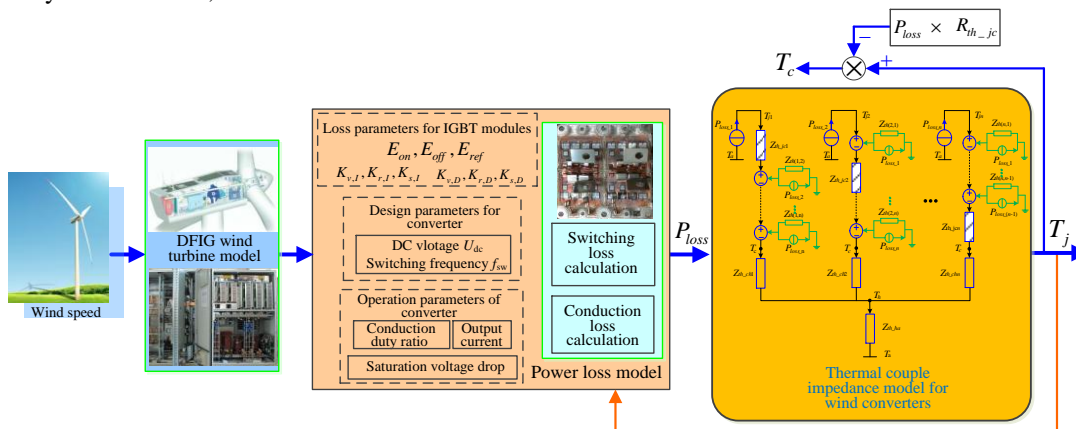

Fig. 13 Flowchart of junction temperature and case temperature calculation of IGBT module for 2MW DFIG wind power converter

As shown in Fig.13, the loss calculation parameters of the multi-chip paralleled IGBT module, i.e. those needed for computing the conduction loss, switching loss, and thermal coupling impedance, can be extracted first according to the datasheet. Then the operational parameters of the converter can be obtained based on the wind speed profile and the DFIG wind turbine model. The power losses of wind power converter can also be calculated during different operation conditions in the light of equations(17)-(21). At last, based on the improved multi-chip thermal coupling model, the junction temperatures

of the chips can be obtained in PLECS simulation. Moreover, the case temperature of the multi-chip paralleled IGBT module can also be obtained.

V. SIMULATION AND PRELIMINARY TESTING

A. Comparison of thermal performances at the rated operation of wind turbine

When the DFIG wind turbine is operated at the rated wind speed of 12 m/s, the junction temperature T_j of chips T2 and D2

in both RSC and GSC are calculated using the traditional model and the proposed model. The results are shown in Fig. 14.
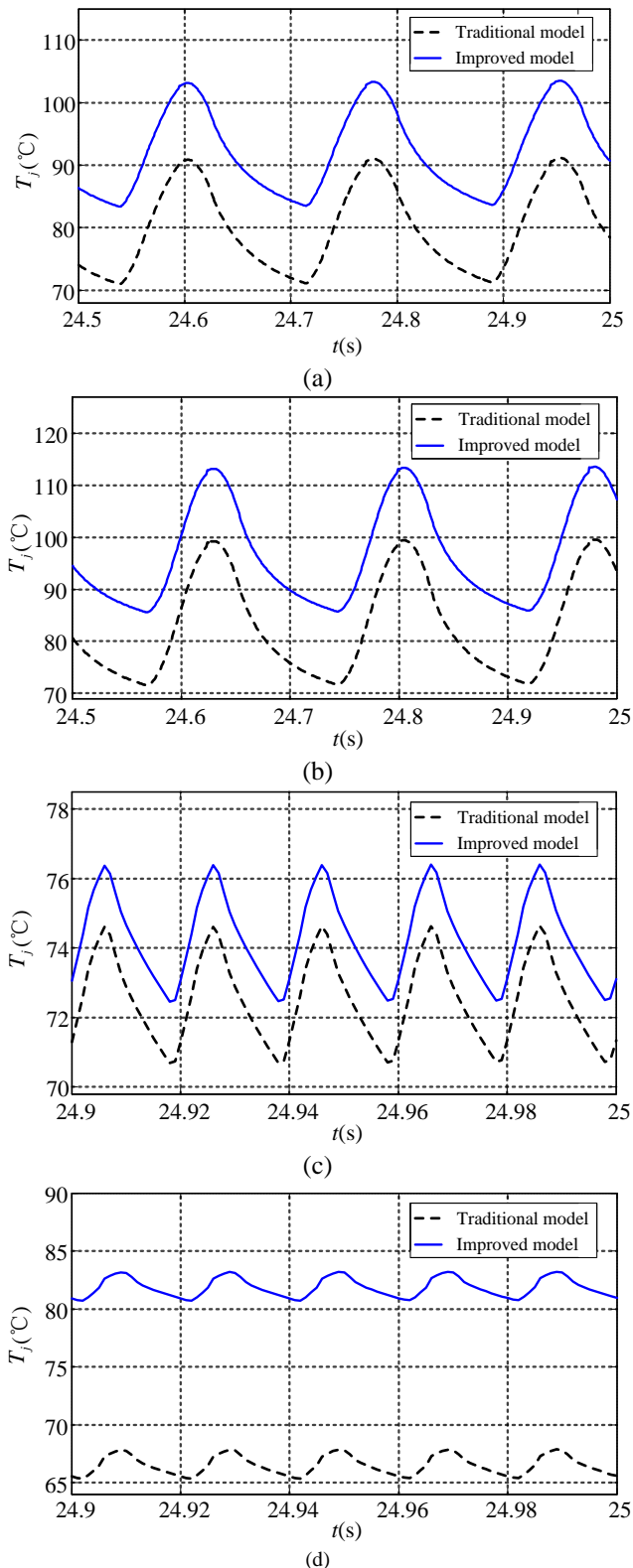

(a)

(b)

(c)

(d)

Fig. 14 Junction temperature of IGBT module for RSC and GSC: (a) for IGBT of RSC, (b) for FWD of RSC, (c) for IGBT of GSC, (d) for FWD of GSC

In Fig.14, it can be seen that the junction temperature T_j obtained by the improved model is again higher than that obtained by the traditional model for both RSC and GSC. This confirms that it is necessary to include the thermal coupling effect for junction temperature calculation of the multi-chip paralleled IGBT module. In the GSC, the effect of coupling on junction temperature obtained from the improved model for FWD is much more significant than for the IGBT. The difference is about 15 ℃ for the former and 2 ℃ for the latter. The main reason is that the GSC is in inverter mode when the DFIG wind turbine is at the rated wind speed condition and the impact of thermal coupling effects of IGBT on FWD is much obvious due to the larger duty and power loss of the IGBT. Moreover, because of different power losses in GSC and RSC, the junction temperatures in the GSC and RSC are quite different. In addition, the fluctuation of junction temperatures is also different in GSC and RSC and more significant in RSC, which perhaps shows that device reliability in RSC needs more attentions.

In the installed wind turbine, direct measurement of the junction temperatures of the multi-chip paralleled IGBT module in the converter is impossible, due to the sealed module packaging, while the case temperature T_c could be acquired easily via SCADA monitoring data. Fig. 15 shows the steady-state case temperature of the module obtained by the traditional model, improved model and the SCADA monitoring as a function of average wind speeds over the wind speed range from 3.99 m/s to 12.05 m/s.

It can be seen that T_c shows a very small increase from 3.99 m/s to 8.17 m/s wind speeds and then a rapid increase with further increase of the wind speed to a saturation level, as the wind speed attains the rated value. The error of T_c of the improved model is much smaller than that of the traditional model. For example, when wind speed is 8.17 m/s, the value of T_c on SCADA monitoring is 52.5 ℃, while 51.5 ℃ and 48.5 ℃ are achieved by the improved model and the traditional model with a difference of 1.9% and 7.6% respectively. The comparisons show the improved model gives higher accuracy calculation results for case temperature because the inclusion of the coupling effect permits the improved model to more accurately predict the increase of power losses at an increased temperature. This indirectly demonstrates that the improved junction temperature modeling and the thermal coupling analysis could be correct.
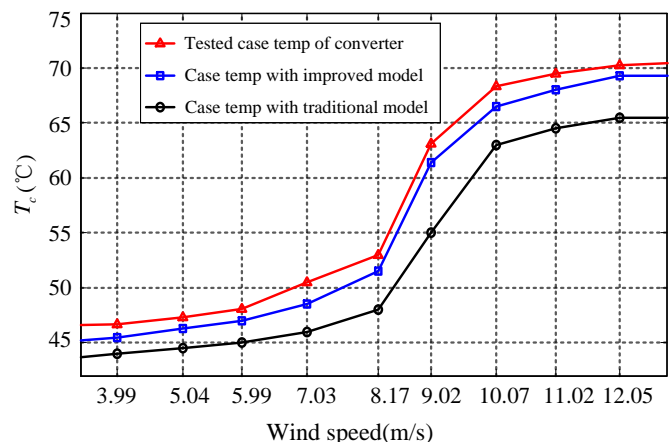

Fig. 15 Tested and simulated results of case temperature of power converter module for 2 MW DFIG at the overall wind speed condition

B. Power loss and coupling junction temperature analysis of IGBT module

When wind speeds are different, the power losses of IGBT modules for RSC and GSC are shown in Fig. 16. The coupling junction temperature as a function of the wind speed is shown in Fig. 17.
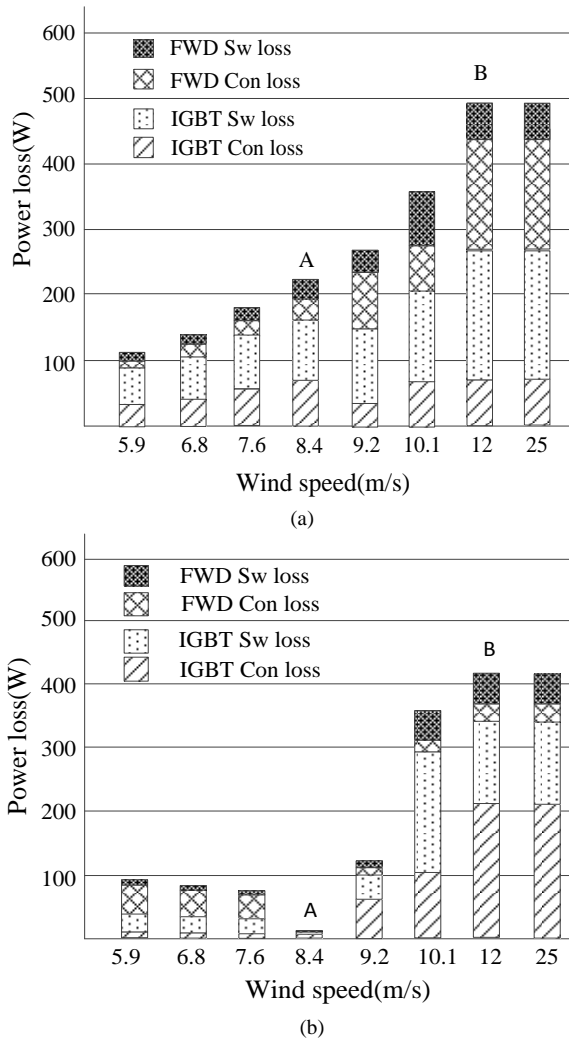

Fig. 16 Power losses of IGBT module of wind turbine power converter at different wind speed points: (a) power losses of IGBT module in the RSC and (b) power losses of IGBT module in the GSC
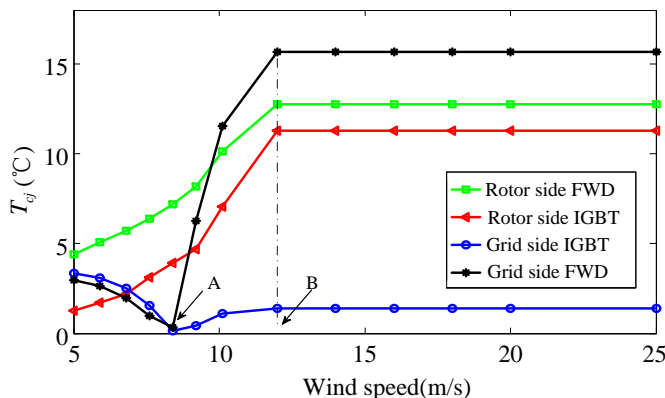

Fig. 17 The coupling junction temperature of IGBT modules of wind turbine power converter at different wind speeds

It can be seen in Fig.16(a) that, for the RSC, the total power loss of IGBT modules increase with wind speed before point B named the rated wind speed point, and the loss remains constant beyond point B. Moreover, before point A at which the system operates at the synchronous speed, the total power loss of IGBT is larger than that of FWD, but there is no significant difference after point A. In Fig.16 (b), for the GSC, it is seen that the total power loss of the IGBT modules decreases before point A and then increase to a saturation level, which is very different compared to the RSC. The junction temperature profiles previously shown in Fig. 15 are similar to the power loss of IGBT modules. Because the junction temperature is related to the power loss, which is different in the GSC and RSC, the junction temperatures are different. Thus, although the DFIG operates under the same condition, such as point A as shown in Fig.17, the junction temperatures in the GSC and RSC are also different because of the difference of power loss in the two converters. In addition, either in the GSC or RSC, the predicted junction temperature with the coupling effect reaches maximum value at the rated wind speed.

It is shown that the thermal coupling effect should not be ignored in junction temperature calculation for multi-chip paralleled IGBT modules. The impact of the thermal coupling effect is much higher for the RSC than the GSC, understanding this may help to improve the control strategy of the RSC for reliability, to adopt a customized IGBT module or to enhance the layout of the multiple chips, like the staggered arrangement of IGBT and FWD.

VI. CONCLUSION

The thermal coupling phenomenon between adjacent chips is analyzed using FEM for a real multi-chip paralleled IGBT module (FZ1600R17HP4) used widely in 2 MW DFIG wind turbines. It is shown that the effect of thermal coupling on junction temperature is glaringly obvious. Based on the thermal coupling effects, an improved junction temperature calculation model with added thermal coupling impedance is proposed. The decrease of the thermal coupling impedance has been shown to be approximately exponential with the distance. Simulation and test results illustrate that the presented model is more valid than the traditional model in terms of the calculation of junction temperature of chips in multi-chip paralleled IGBT modules. According to the presented model, the junction temperatures of chips in the GSC and RSC of a 2 MW DFIG wind turbine are calculated, which are quite different because of the difference of power loss in GSC and RSC. It is also shown that the thermal coupling effect on the FWD is more obvious than IGBT above the rated wind speed, either for the GSC or RSC. The proposed model and the results obtained are important for reliability evaluation and condition monitoring of the wind turbine power converter, as well as other multi-chip paralleled power electronic systems.

REFERENCES

[1] H. Packard, "A guide to understanding, measuring, and applying power FET thermal resistance coefficients," *High-frequency transistor primer part III-A: thermal resistance.*

This article has been accepted for publication in a future issue of this journal, but has not been fully edited. Content may change prior to final publication. Citation information: DOI 10.1109/TEC.2016.2614526, IEEE Transactions on Energy Conversion

10

[2] M. P. Gil, O. G. Bellmunt, and A. Sumper, "Technical and economic assessment of offshore wind power plants based on variable frequency operation of clusters with a single power converter," *Applied Energy*, vol. 125, no. 21, pp. 218-229, Jul. 2014.

[3] S. Yang, D. Xiang, A. Bryant, P. A. Mawby, L. Ran, and P. J. Tavner, "Condition monitoring for device reliability in power electronic converters - a review," *IEEE Trans. Power Electron.*, vol. 25, no.11, pp. 2734-2752, Nov. 2010.

[4] T. Satoshi, M. Kohei, "High junction temperature and low parasitic inductance power module technology for compact power conversion systems," *IEEE Trans. Electron Devices*, vol. 62, no. 2, pp. 258-269, Feb. 2015.

[5] P. M. Fabis, D. Shun, H. Windischmann, "Thermal modeling of diamond-based power electronics package," in *Proc. IEEE Int. Conf. SEMI-THERM Symp.*, Mar. 1999, pp. 98–104.

[6] M. Chen, A. Hu, X. D. Yang," Predicting IGBT Junction Temperature with Thermal Network Component Model," in *Proc. IEEE Int. Conf.*, *Power Energy Engineering*, Asia-Pacific, Mar. 2011, pp. 1-4.

[7] L. X. Wei, R. J. Kerkman, R. A. Lukaszewski, B. P. Brown, N. Gollhardt, B. W. Weiss, "Junction temperature prediction of a multiple-chip IGBT module under DC condition," in *Conf. Rec. IEEE IAS Annu. Meeting*, Oct. 2006, pp. 754-762.

[8] L. B. Zheng, L. Han, X. H. Wen, "Investigation of the Temperature Character of IGBT Failure Mode Based on 3D Thermal-Electro Coupling FEM," *Transactions of China Electro-technical Society*, vol. 26, no.7, pp. 242-246, Jul. 2011.

[9] F. F. Song, X. Q. He, P. Lai, R. Wang, "The Study of infrared radiation thermal imaging technology for temperature testing," in *Proc. IEEE Int. Conf. Electronic Packaging Technology and High Density Packaging*, Aug. 2012, pp. 1336-1339.

[10] W. H. Chen, H. C. Cheng, H. A. Shen, "An effective methodology for thermal characterization of electronic packaging," *IEEE Trans. Compon. Packaging T.*, vol. 26, no.1, pp. 222-232, Jun. 2003.

[11] K. Ma, F. Blaabjerg, M. Liserre, "Thermal analysis of multilevel grid side converters for 10MW wind turbines under low voltage ride through," in *Proc. IEEE ECCE*, Sept. 2011, pp. 2117-2124.

[12] K.Ma, F. Blaabjerg, D. Xu, "Multilevel Converters for 10 MW wind turbines," in *Proc. IEEE Int. Conf. Consumer Electronics Symp.*, Aug. 2011, pp. 340-346.

[13] M. Musallam, P. P. Acarnley, C. M. Johnson, L. Pritchard, V. Pickert. "Estimation and Control of Power Electronic Device Temperature During Operation With Variable Conducting Current," *IET Circuits Devices Syst.,* vol. 1, no. 2, pp. 111-116, Apr. 2007.

[14] Z. J. Qiu, J. Zhang, X. H. Wen, "Evaluation of chip temperature for multichip IGBT modules by using the thermo-sensitive electrical parameter (TSEP)," in *Proc. IEEE Int. Conf. Electrical Machines and Systems*, Oct. 2013, pp.1800-1803.

[15] V. Sundaramoorthy, E. Bianda, R. Bloch, I. Nistor, G. Knapp, A. Heinemann, "Online estimation of IGBT junction temperature (Tj) using gate-emitter voltage (Vge) at turn-off," in *Proc. IEEE EPE*, Sept. 2013, pp. 1-10.

[16] H. Yi-Cheng, L. Yu-Kuan, C. Ming-Hung, T. Chun-Chin, K. Jao-Hwa, H. Sheng-Bang, H. Hung-Lieh, S. Yeh-I, and C. Wood-Hi, "Failure Mechanisms Associated With Lens Shape of High-Power LED Modules in Aging Test," *IEEE Trans. Electron Devices*, vol. 55, no. 2, pp. 689–694, Feb. 2008.

[17] H. Lambate, S. Nakanekar, S. Tonapi,"Thermal characterization of the IGBT modules used in hybrid electric vehicles," in *Proc. IEEE Int. Conf. Thermal and Thermomechanical Phenomena in Electronic Systems*, May. 2014, pp.1086-1091.

[18] Anis Ammous, Sami Ghedira, Bruno Allard, Hervé Morel, and Denise Renault, "Choosing a thermal model for electrothermal simulation of power semiconductor devices," *IEEE Trans. Power Electron.*, vol. 14, no. 2, pp. 300-307, Mar. 1999.

[19] J. Crank, The Mathematics of Diffusion, 2nd ed. Oxford, London, U.K.: Clarendon, 1975.

[20] J. J. Grainger, and W. D. Stevenson, Jr., Power System Analysis, McGraw-Hill Electrical and Computer Engineering Series, 1994.

[21] M. Chinchilla, S. Arnaites, J. C. Burgos, "Control of permanent-magnet generators applied to variable-speed wind-energy systems connected to the grid," *IEEE Trans. Energy Convers.*, vol.21, no.1, pp. 130-135, Mar. 2006.

[22] A. Tapia, G. Tapia, J. X. Ostolaza, J. R. Saenz, "Modeling and control of a wind turbine driven doubly fed induction generator," *IEEE Trans. Energy Convers.*, vol.18, no.2, pp. 194-204, Jun. 2003.

[23] L. Y. Wu, J. C. Qin, M. Saeedifard, O. Wasynczuk, K. Shenai, "Efficiency Evaluation of the Modular Multilevel Converter Based on Si and SiC Switching Devices for Medium/High-Voltage Applications," *IEEE Transactions on Electron Devices*, vol.62, no.2, pp. 286-293, Feb. 2015.

Hui Li received the M. Eng. degree and the Ph. D degree in electrical engineering from Chongqing University, Chongqing, China, in 2000 and 2004, respectively. He was a Postdoctoral Research Fellow at the Institute of Energy Technology, Aalborg University, Denmark, in 2005-2007. Since 2008, he has been a professor with the Department of Electrical Machinery and Electrical Apparatus, School of Electrical Engineering of Chongqing University. Currently, he is also a researcher with the State Key Laboratory of Equipment and System Safety of Power Transmission and Distribution & New Technology. His main research areas include wind power generation, design and control of electrical machines.

Xinglin Liao received the M.S. degree from Southwest Jiaotong University, Chengdu, China, in 2012. He is current pursuing the Ph.D. degree in electrical engineering in the School of Electrical Engineering, Chongqing University, Chongqing, China. His research interests include wind power generation converter, thermal analysis and the application of SiC power electronics.
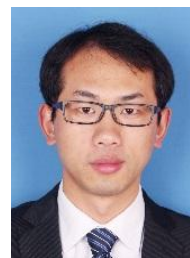
Zheng Zeng received the Ph.D degree in electrical engineering from the Department of Electrical Engineering, Zhejiang University, Hangzhou, China, in 2014. He is currently a Lecturer in the School of Electrical Engineering, Chongqing University, Chongqing, China. His research interests include multi-functional grid-connected inverter for renewable energy integration and customized package for wideband gap power electronic devices.

Yaogang Hu received the B.S. and M.S. degrees in electrical engineering from the Yanshan University and Chongqing University, China, in 2008 and 2011. Currently, he is working toward the Ph.D. degree in electrical engineering at the Chongqing University, Chongqing, China. His research interests include condition monitoring, fault diagnosis, and lifetime prediction for wind turbine.

This article has been accepted for publication in a future issue of this journal, but has not been fully edited. Content may change prior to final publication. Citation information: DOI 10.1109/TEC.2016.2614526, IEEE Transactions on Energy Conversion

11

Yang Li received the M.S. degrees in electrical engineering from the Chongqing University, Chongqing, China, in 2016. Currently, he works in State Grid Chongqing Electric Power Co. Electric Power Research Institute, Chongqing, China. His research interests include thermal management of power electronics devices used in wind power converter.

Shengquan Liu received the M.S. degrees in electrical engineering from the Chongqing University, Chongqing, China, in 2015. Currently, he is working in State Grid Jiangxi Electric Power Corporation Ganzhou Power Supply Company. His research interests include IGBT model, junction temperature calculation and converter reliability estimation.

Li Ran (M'98-SM'07) received a PhD degree in Power Systems Engineering from Chongqing University, Chongqing, China, in 1989. He was a Research Associate with the Universities of Aberdeen, Nottingham and Heriot-Watt, at Aberdeen, Nottingham and Edinburgh in the UK respectively. He became a Lecturer in Power Electronics with Northumbria University, Newcastle upon Tyne, the UK in 1999 and was seconded to Alstom Power Conversion, Kidsgrove, the UK in 2001. Between 2003 and 2012, he was with Durham University, the UK. He joined the University of Warwick, Coventry, the UK as a Professor in Power Electronics - Systems in 2012. His research interests include the application of Power Electronics for electric power generation, delivery and utilization.